Korean J. Chem. Eng., **18**(6), 809-815 (2001)

Characteristics of Transient Blood Flow in MHVs with Different Maximum Opening Angles using Fluid-Structure Interaction Method

Choeng-Ryul Choi†, Chang-Nyung Kim* and Myung-Jin Choi*

Department of Mechanical Engineering,*College of Mechanical and Industrial System Engineering,
Kyunghee University, Yong-in, Kyung-gi 449-701, Korea
(*Received 17 January 2001 • accepted 26 June 2001*)

Abstract—A numerical analysis has been performed to investigate the characteristics of two-dimensional transient blood flows interacting with the leaflet motion in a bileaflet mechanical heart valve with different maximum opening angles, located in the aortic position. Here, for one cycle of heartbeat the analysis has been carried out in the light of fluid-structure interaction since the blood flow and the leaflet motion are coupled with each other. Blood has been assumed to be a Newtonian and non-Newtonian fluid, where the Carreau model has been used for the simulation of non-Newtonian fluid. Physiologic ventricular and aortic pressure waveforms have been used as flow boundary conditions at the ventricle and the aorta. A finite volume computational fluid dynamics code and a finite element structure dynamics code have been used concurrently to solve the flow and the structure equations, respectively, where the two equations are strongly coupled. Flow fields, leaflet behavior, and shear stresses with time have been obtained. Also the discharge and the regurgitation flow rates have been calculated. The maximum shear stress, an important issue for valve hemodynamic analysis, has been found in the vicinity of the contact point where a leaflet contacts with housing in the final stage of the closing phase.

Key words: Mechanical Heart Valve (MHV), Hemodynamics, Fluid-Structure Interaction, Blood Flow, Pulsatile Flow, Shear Stress

INTRODUCTION

A heart is a two-sided pump responsible for circulating blood throughout a body. Inside a heart in a human body there are four chambers and each side has two of them. The upper chambers are called the atria, and the lower chambers are the ventricles. A heart has four different cardiac valves: tricuspid valve (right atrium-right ventricle), pulmonary valve (right ventricle-pulmonary artery), mitral valve (left atrium-left ventricle) and aortic valve (left ventricle-main artery). The four valves act as one-way doors between the chambers. These valves allow forward flow and prevent backflow of blood moving through the heart.

Healthy valve leaflets are formed from thin and pliable tissues that open and close as the heart contracts and relaxes. However, heart valves can be abnormally formed congenitally. And they can be damaged or scarred by rheumatic fever, infection, inherited conditions, aging and heart attacks. The aortic and mitral valves are the ones most often affected. Abnormal heart valves will cause the heart to work harder to pump the required amount of blood through the body. This excess work can weaken the heart, causing it to enlarge and incur various symptoms. Some of these symptoms include chest pain, shortness of breath, dizziness, fainting, chronic tiredness, and swelling of the feet and legs.

In some cases it is possible to repair a valve by performing a surgical procedure called valvotomy, valvuloplasty, or valve repair. But if a valve is so seriously deformed or diseased, it must be removed and replaced with a prosthetic (artificial) heart valve. There are two main types of artificial valves: bioprostheses and mechanical valves. Firstly, bioprostheses or bioprosthetic valves are made of biological tissue (human or treated animal tissues). Secondly, mechanical valves are made of metal, carbon, and/or synthetics. Bileaflet mechanical heart valves (MHV) are the most commonly implanted prosthetic heart valves (Fig. 1). Although these valves are durable, patients require anticoagulation therapy to prevent thrombosis and thromboembolism.

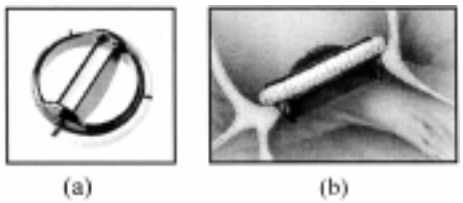

Fig. 1. Bileaflet mechanical heart valve (MHV).
(a) bird's-eye view, (b) side view of installed MHV in the aorta

When the valve is fully opened, high velocity jets through the gap between the leaflets can be readily detected both *in vivo* and *in vitro* [Chandran, 1985a; Woo et al., 1986; Hasenkam et al., 1988; Nygaard et al., 1994]. The leaflets act as an obstruction to the blood flow through the valve and this, coupled with the high velocity jets through the leaflets, causes elevated shear stresses which may cause red blood cell damage or platelet activation [Hasenkam et al., 1988; Hung et al., 1976; Leverett et al., 1972; Woo et al., 1986]. Together with high shear stress, increased coagulation caused by blood stagnancy in contact with the artery walls may yield thrombosis and thromboembolism, which should be avoided in patients with a prosthetic heart valve implant. An improvement of valve design requires

†To whom correspondence should be addressed.
E-mail: crchoi@cvs2.kyunghee.ac.kr

a detailed understanding of these system properties and further substantial research. Analysis of the flow field around the valve may identify the areas of flow disturbance and the areas of stasis close to the valve, and this information can then be used to improve current valve designs.

Most of the research has been performed through *in vitro* experimental studies since *in vivo* experimental investigations are extremely difficult. Although many important aspects of hemodynamic aortic blood flow have been investigated in experimental studies [Sallam et al., 1976; Yoganathan et al., 1979; Skalak et al., 1982; Rossean et al., 1984; Tillman et al., 1984; Chandran et al., 1985b, c; Farahifar et al., 1985; Gross et al., 1988, Fatermi et al., 1989; Sikarskic et al., 1979], they lack spatial resolution, have problems analyzing transient phenomena or partially lack the detailed observation of theoretically interesting variables crucial for extended theoretical modeling because it is difficult to measure them.

Analysis of computational fluid dynamics (CFD) is an alternative tool that can be used to investigate the complex flow patterns within the valve and the flow downstream of heart valves. Once a CFD model is defined and validated, small changes can be made to one design parameter, such as the leaflet-opening angle, and the effect of this alteration on the flow field can be thoroughly investigated.

Many researchers have performed investigations on the flow field around the bileaflet mechanical heart valves using CFD analysis [McQueen et al., 1985; Stevenson et al., 1985; King, 1994; King et al., 1994; Cerrolaza et al., 1997; Krafczyk et al., 1998; Gokhale et al., 1978; Imaeda et al., 1980]. Previous studies have either ignored the effects of valve leaflet motion or approximated it using simplified assumptions, although the bileaflet mechanical heart valve cyclically performs an open-and-close process by the heartbeat. Therefore, they cannot have depicted clearly the flow field and the leaflet motion for a complete cardiac cycle. To obtain reliable results, fluidstructure interaction between the blood flow and the leaflets motion has to be included.

The aim of this paper is to overcome the shortcomings of previous studies where the leaflet motion has been ignored or simplified, and to investigate the characteristics of the blood flow and the leaflet motion in the bileaflet mechanical heart valves in the aortic position by fluid-structure interaction analysis. In this study two-dimensional, pulsatile flows have been simulated in the valves with different maximum opening angles. A finite volume computational fluid dynamics code and a finite element structure dynamics code have been used concurrently to solve the flow and structure equations, respectively, to investigate the interaction between the blood flow and leaflet. Blood has been assumed to be a non-Newtonian and Newtonian fluid with Carreau model. All calculations have been performed for one cycle of heartbeat.

MATHEMATICAL MODELING

The governing equations for fluid and structure have been considered simultaneously to obtain the flow field and the leaflet behavior for an open-and-closed cardiac cycle. The following are assumed to simplify the governing equations: The blood is a homogeneous incompressible fluid. The density of fluid is constant and the flow is laminar [Jeong et al., 1995].

1. Governing Equations for Blood Flow

The governing equations for blood flow are the continuity equation and the Navier-Stokes equation for an incompressible fluid, which can be written in a strong conservation form in curvilinear coordinates as follows:

$$\frac{\partial}{\partial t}\left(\frac{\rho}{J}\right)+\frac{\partial}{\partial \xi^j}\left(\frac{\rho U_j}{J}\right)=0 \tag{1}$$

$$\frac{\partial}{\partial t}\left(\frac{\rho u_i}{J}\right)+\frac{\partial}{\partial \xi^j}\left(\frac{\rho U_j u_i}{J}\right)=-\frac{1}{J}\frac{\partial \xi^j}{\partial x_i}\frac{\partial p}{\partial \xi^j} +\frac{\partial}{\partial \xi^k}\left[\frac{\mu}{J}\frac{\partial \xi^k}{\partial x_j}\left(\frac{\partial \xi^l}{\partial x_j}\frac{\partial u_i}{\partial \xi^l}+\frac{\partial \xi^l}{\partial x_i}\frac{\partial u_j}{\partial \xi^l}-\frac{2}{3}\delta_{ij}\frac{\partial u_l}{\partial \xi^m}\frac{\partial \xi^m}{\partial x_l}\right)\right] \tag{2}$$

where u_i is the Cartesian velocity component, x_i is the Cartesian coordinate, U_j is the velocity component in the ξ^j direction (contravariant velocity component), and J is the coordinate transformation Jacobian. Further,

$$x_1=x,\ x_2=y,\ x_3=z,\ \xi^1=\xi,\ \xi^2=\eta,\ \xi^3=\zeta \tag{3}$$

$$U_j=\frac{\partial \xi^j}{\partial t}+\frac{\partial \xi^j}{\partial x_i}u_i=0 \tag{4}$$

where, $\partial\xi^j/\partial t$ represents the grid velocity, so that the above formulation is in an Eulerian-Lagrangian frame.

2. Governing Equation for Structural Dynamics

The finite element formulation of the structural dynamics equation can be generally written in a linear form as follows:

$$[M]\{\ddot{q}\}+[C]\{\dot{q}\}+[K]\{q\}=\{F\} \tag{5}$$

where {q}, [M], [C], [K] and {F} are the displacement vector, the mass matrix, the damping matrix, the stiffness matrix, and the force vector caused by the fluid dynamic load and shear stresses, respectively.

$$[M]=\sum m_{ij}^e=\sum\int N_i\rho_s N_j dv \tag{6-a}$$

$$[C]=\sum C_{ij}^e=\sum\int N_i\mu_s N_j dv \tag{6-b}$$

$$[K]=\sum k_{ij}^e=\sum\int B_i D_{ji} B_i dv \tag{6-c}$$

$$\{F\}=\sum\{f_i\}^e=\sum\int N_i dp v \tag{6-d}$$

where N_i, ρ_s, μ_s and D_{ij} are the shape function, the density of the structure, the damping parameter and the elasticity matrix. B_i is related to N_j through a linear operator;

$$B_i=L_{ij}N_j \tag{7}$$

Newmark's scheme is applied to solve the above Eq. (5). For known values of q, $\dot{q}$, $\ddot{q}$ at (n−1)th time step, we have

$$\{q\}=\frac{2}{\Delta t}\left[[k]+\frac{4}{\Delta t^2}[M]+\frac{4}{\Delta t}[C]\right]^{-1}\{F\}+\{E\} \tag{8}$$

where {E} comprises all the terms of q^{n-1}, $\dot{q}^{n-1}$ and $\ddot{q}^{n-1}$.

3. Coupling of Fluid and Structure

In Eq. (2) of fluid dynamics, the structural effect comes into play only through the grid velocity term. This section will discuss the implicit coupling procedure. It is known that at the fluid-structure interface, fluid velocity is always equal to the structure velocity and

the contravariant velocity component in the Eulerian-Lagrangian formulation is zero:

$$U_j = \frac{\partial \xi^j}{\partial t} + \frac{\partial \xi^j}{\partial x_i} u_i = 0 \quad (4)$$

If $\{q\}_b$ is the velocity of structure at the fluid-structure interface, then

$$\{\dot{q}\}_b = -\frac{\partial \xi^j}{\partial t} = \frac{\partial \xi^j}{\partial x_i} u_i \quad (9)$$

On the other hand, Eq. (8) can be expressed in the following perturbation form:

$$\{\dot{q}\}'_b = [IC]\{p\}'_b \quad (10)$$

In view of Eq. (9), we have

$$\frac{\partial \xi^j}{\partial x_i} u'_i = [IC]\{p\}'_b \quad (11)$$

where [IC] and $\{p\}_b$ are the influence coefficient [Yang et al., 1994] and the pressure at the fluid-structure interface, respectively. When Eq. (11) is substituted into the pressure gradient term of the pressure correction equation, the resulting equation depends only on flow variables.

In the process of numerical calculation fluid velocities and pressures are computed at each time step solving the Navier-Stokes momentum and continuity equations. The fluid and structural dynamics models and the fluid-structure interaction method are embedded in the iterative procedure. In the process of the fluid-structure interaction fluid forces on the valve are used to compute leaflet motion during each iteration. On the contrary, the leaflet surface velocity is imposed on the fluid in the altered flow domain during the next iteration, which means that the fluid-structure interface is moving. Fluid velocities and pressures are once again computed and the updated fluid forces on the leaflet are applied as boundary conditions of the structure (leaflet). This process continues until both the flow variables and structural behavior converge to equilibrium values. The numerical computation then proceeds to the next time step and the entire procedure is repeated. The rigorous scheme ensures fully coupled flow and structural solutions at each time step. A time accurate, backward Euler, upwind differencing SIMPLEC scheme has been used in the flow solver.

NUMERICAL ANALYSIS

Using the fluid-structure interaction method, two-dimensional pulsatile blood flows interacting with the leaflet motion have been analyzed numerically in bileaflet mechanical heart valves (St. Jude Medical) installed in aortic position. Although the MHV is geometrically three-dimensional, the blood flow has been assumed to be two-dimensional since the two leaflets of the MHV are of plane shape and the calculation for three-dimensional transient simulation requires a considerable amount of calculation time. We will handle the analysis for three-dimension geometry later. Investigation has been carried out with the governing equations for blood flow and leaflet behavior, respectively, together with an auxiliary equation which is coupled with the above equations. To solve these equations, a commercial software package CFD-ACE+ ver. 6.4 and FEMSTRESS (add-on module for CFD-ACE; a finite element structural analysis module) have been adopted.

Table 1. Classification of the calculated cases

Classification	Fluid	Opening angle
case 1	Newtonian fluid	25°≤θ≤75°
case 2	Newtonian fluid	25°≤θ≤80°
case 3	Newtonian fluid	25°≤θ≤85°
case 4	Non-Newtonian fluid	25°≤θ≤85°

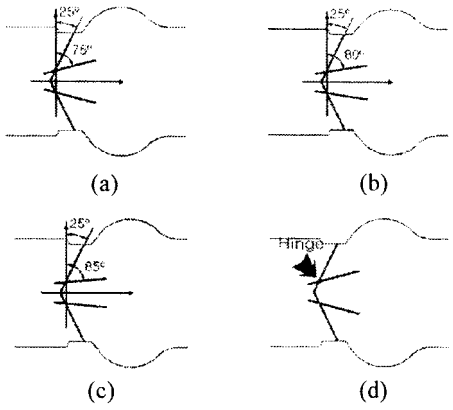

Fig. 2. Opening angles in different cases and hinge point.
(a) case 1 (25°≤θ≤75°), (b) case 2 (25°≤θ≤80°), (c) case 3 (25°≤θ≤85°), (d) Hinge point

Calculations for four cases have been carried out as shown in Table 1. In cases 1~3, the blood has been assumed to be Newtonian fluid and the opening angles have been set to be 25°≤θ≤75°, 25°≤θ≤80° and 25°≤θ≤85°, respectively. Detailed figures of the different leaflet-opening angles in these cases are shown in Fig. 2. Hinge point meaning rotation axis of leaflet is denoted in Fig. 2(d). The actual angle of closure becomes not θ_{min}=25° but θ_{min}=26° since the gap (70 μm) between the leaflet and housing exists when the leaflet is fully closed. Therefore, reverse flow (leakage flow) toward ventricle is caused when the leaflet is closed.

For Newtonian fluid, in the cases 1~3 the density ρ is 971 kg/m^3 and the dynamic viscosity μ is 3.5×10^{-3} kg/m·s. The case 4 has been considered with the opening angle 25°≤θ≤85° and with non-Newtonian fluid of the Carreau model as follows:

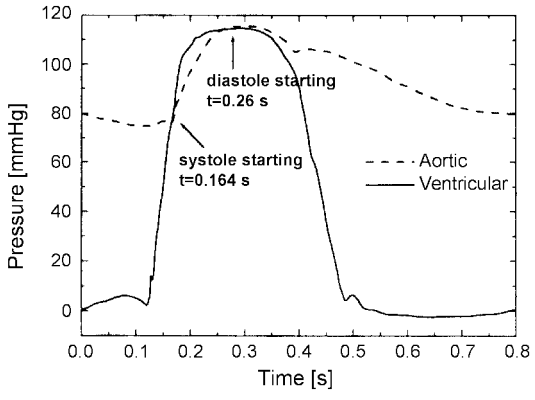

Fig. 3. Pressure waveforms used as the boundary conditions.

$$\mu = \mu_\infty + (\mu_0 - \mu_\infty)\cdot[1+(K\dot{\gamma})^a]^{n-1/a} \quad (12)$$

where μ_0=0.1072 kg/m·s, μ_∞=3.5×10^{-3} kg/m·s, n=0.3568, K=2.6502, a=2, and the shear rate $\dot{\gamma}=\left(\frac{\partial u}{\partial y}+\frac{\partial v}{\partial x}\right)$. The density is the same as that of a Newtonian fluid.

The diameter of an aortic blood vessel has been assumed to be 27.0 mm. The geometry of the downstream region of MHV has been adopted from the Sinus of Valsalva model suggested by Swanson et al. [1974]. The pressure waveforms, measured *in vitro* [Thubrikar et al., 1996a, b] in the ventricle and the aorta with 75 beats per minute, have been used as pressure boundary conditions for the numerical calculation (Fig. 3). At the vessel surface no slip condition has been given for the blood flow and at the leaflet surface the velocity of the blood is identical to that of the leaflet surface. The current numerical calculation has included 9114 cells and has employed the time step of 0.0005s. It has taken about 70 hours (in each case) to converge with a PC of Pentium III 800 and 512MB RAM.

RESULTS AND DISCUSSION

Velocities fields and shear stress contours in three different cases are depicted in Fig. 4. In each plot velocity fields are described in the upper part and the shear stress in the lower part. The leaflet mo-

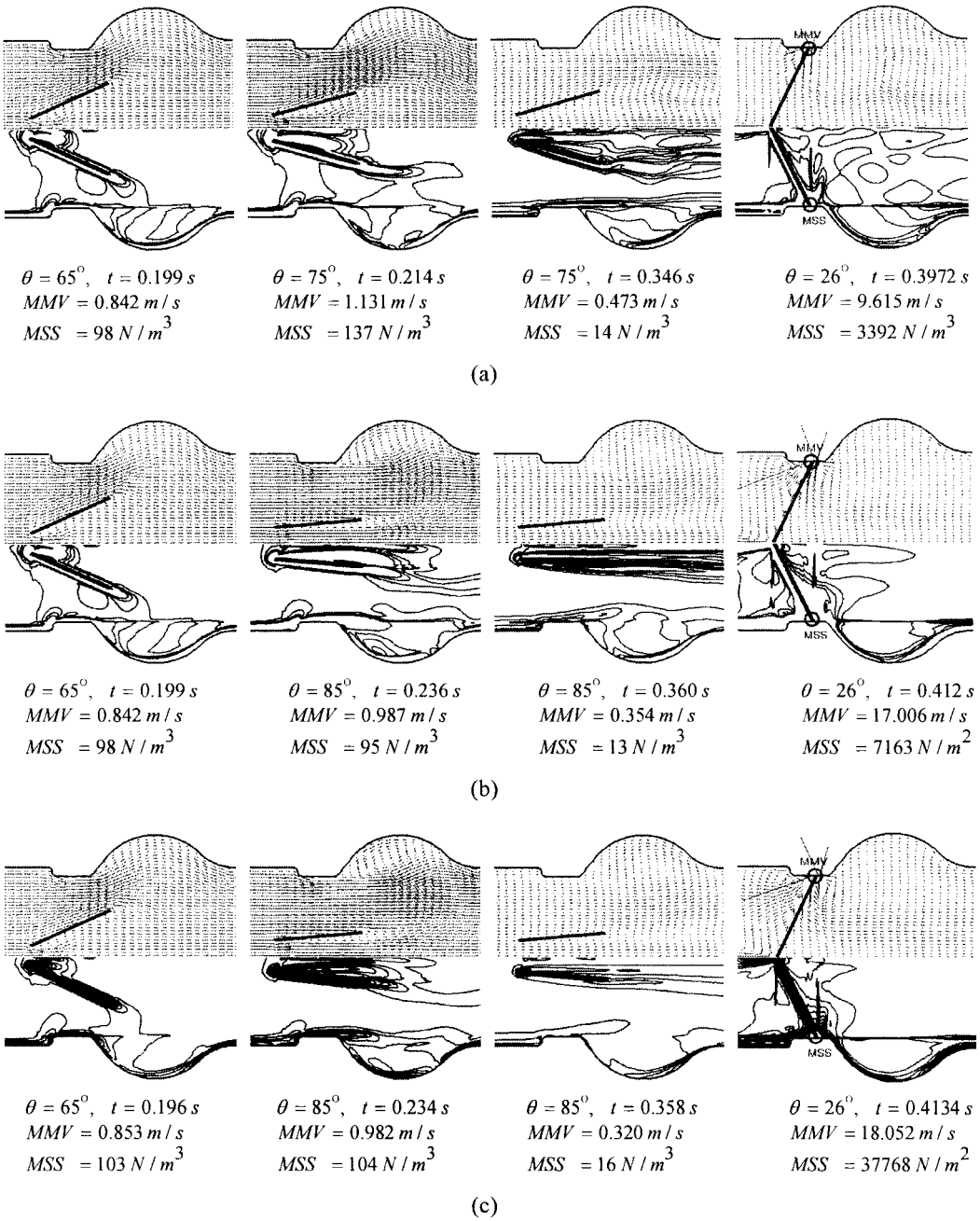

Fig. 4. Velocity fields and shear stress contours (MMV: Magnitude of maximum velocity, MSS: Maximum shear stress).
(a) case 1 (25°≤θ≤75°, Newtonian fluid), (b) case 3 (25°≤θ≤85°, Newtonian fluid), (c) case 4 (25°≤θ≤85°, non-Newtonian fluid)

tion can be divided into four durations: opening phase, opened phase, closing phase and closed phase. Plots in the figure, from the left to the right, correspond to the opening phase, the end stage of opening phase arriving at the maximum opening angle, the end stage of opened phase meaning the starting point of closing phase and the final stage of closing phase, respectively. In the opening phase (the first column) of the three cases, the flows between a leaflet and housing, having almost uniform velocities, are faster than those between the two leaflets. This is different from the result of other researchers who reported three jet-like fast flows found downstream of the leaflets on the assumption of ignored or simplified leaflets motion.

In the second column, the stream of outer side of the two leaflets in the case 1 with θ_{max}=75° tilts toward the sinus cavity more than that in the case 3 with θ_{max}=85°. Because of large maximum opening angle, the flow in the case 3 results in larger recirculation in the sinus cavity compared with the case 1. In the third column, reverse flows start to occur downstream of the leaflet and propagate to the whole flow domain associated with the ventricular diastole. The starting time of the closing phase in the case 1 with θ_{max}= 75° is 0.348 s, and that in the case 3 with θ_{max}=85° is 0.354 s. This shows that the smaller the maximum opening angle is, the earlier the closing phase starts.

In the final stage (the fourth column) of the closing phase, jet-like flow is found between the leaflet and housing (marked in the figure) in all the cases. The magnitudes of the maximum velocity (MMV) in this region are denoted in the figure. Here, the magnitude of the maximum velocity in the final stage of the closing phase is immensely larger than that of other phases. The flow fields for Newtonian and non-Newtonian fluid are similar to each other.

The extent of blood cell damage is a function of both the magnitude of shear stresses acting on blood corpuscles and their exposure time to shear fields. Furthermore, platelets have a lower tolerance to shear stress compared to red blood cells. Therefore, damage to these platelets caused by shear stress may be an important factor for the initiation of thromboembolic complications. The magnitudes of the shear stress (MSS) have been calculated and depicted in the figure. In the final stage of the closing phase an immensely large value of maximum shear stress is found in the vicinity of the contact point where a leaflet contacts with the housing. Especially, for non-Newtonian fluid the maximum shear stress is much larger than that of a Newtonian fluid. Note that both the position and the time corresponding to the maximum shear stress in the flow field during one cycle are exactly identical to those corresponding to the maximum velocity.

Changes in leaflet angle, leaflet angular velocity, blood flow rate, the maximum velocity and maximum shear stress in the blood flow during one cycle are shown in Fig. 5. The pressure waveform adopted for boundary conditions given in Fig. 3 is shown again in Fig. 5(a) for the convenience of comparison. The ventricle systole starts at t=0.164 s and the ventricle diastole at t=0.26 s. Variations of the opening angle and the leaflet angular velocity are shown in Fig. 5(b) and Fig. 5(c).

The smaller the maximum opening angle is, the earlier the closing phase is started and finished. The closing phase in case 1 is 0.346 s≤ t≤0.397; in case 2, 0.357 s≤t≤0.405; in case 3, 0.360 s≤t≤0.412; in case 4, 0.358 s≤t≤0.413. When the leaflet starts to contact with the housing, a small bounce of the leaflet takes place because of the

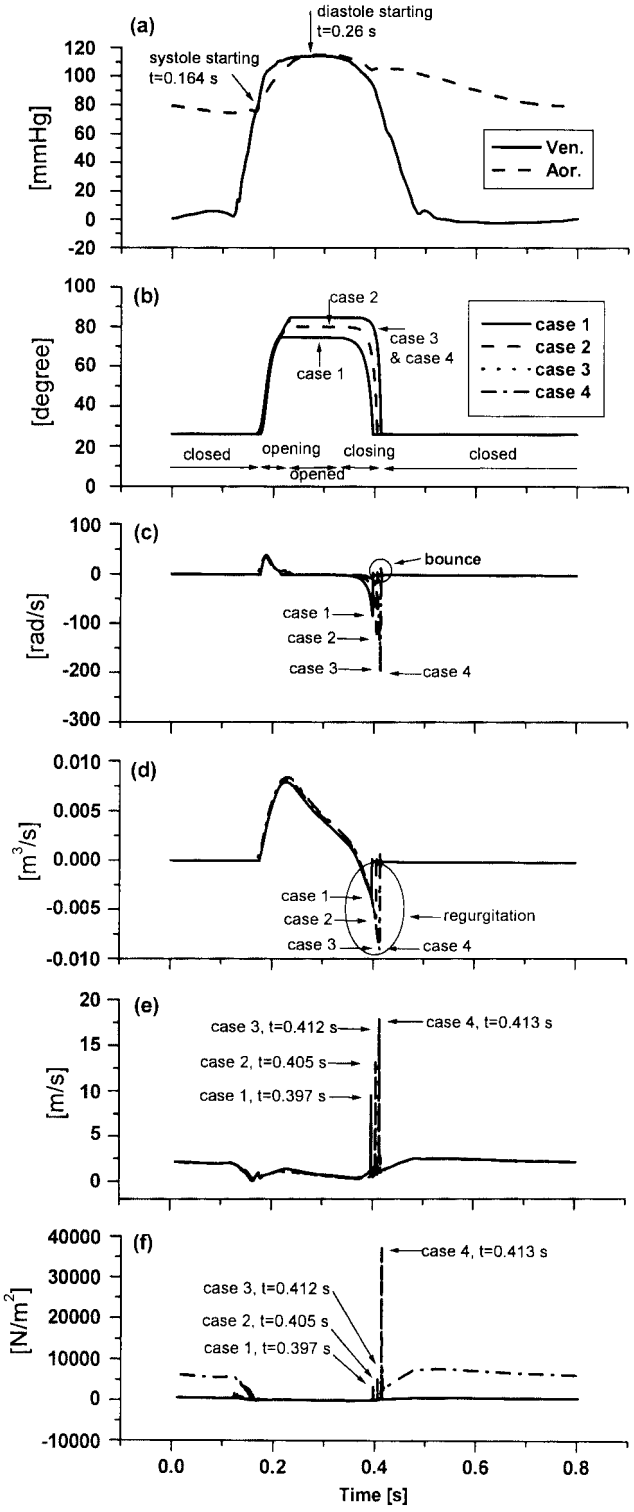

Fig. 5. Leaflet behavior, flow rate, and the maximum velocity and shear stress.
(a) Pressure waveforms of ventricle and aorta, (b) Leaflet opening angle, (c) Leaflet angular velocity, (d) Volumetric flow rate, (e) Maximum velocity, (f) Maximum shear stress

inertia effect of the leaflet motion (Fig. 5c). Although the ventricle diastole starts at t=0.26 s, the closing phase starts later. It can be noted that there is a time delay between the ventricle diastole and

Table 2. Blood flow rate per one cycle [unit : m^3/s]

	Q_{dis}	Q_{reg} ($Q_{reg}/Q_{dis} \times 100\%$)	Q_{net}
Case 1	8.868e-04	0.513e-04 (5.8%)	8.355e-04
Case 2	9.336e-04	0.886e-04 (9.5%)	8.450e-04
Case 3	9.549e-04	1.425e-04 (14.9%)	8.126e-04
Case 4	9.920e-04	1.500e-04 (15.1%)	8.418e-04

Q_{dis}: discharge flow rate, Q_{reg}: regurgitation flow rate, Q_{net}: net flow rate.

the start of closing phase in all cases. The angular velocity of the leaflet at the final stage of the closing phase is considerably larger than that of the opening phase in all cases. The larger the maximum opening angle of the leaflet is, the faster the angular velocity of leaflet is in the closing phase. The leaflet behaviors in Newtonian and non-Newtonian cases are generally similar to each other.

Volumetric flow rates have been calculated and shown in Fig. 5(d). The flow rates increase rapidly with ventricle systole and decrease slowly with ventricle diastole. Reverse flow named "closing regurgitation" exists during the closing phase. Discharge flow rates, closing regurgitation flow rates and net flow rates during one cycle have been shown in Table 2. Although the discharge flow rate in case 3 is the largest of all the cases, the net flow rate, Q_{net} in case 2 is the largest because the closing regurgitation flow rate is fairly large in case 3. The profiles of the maximum velocity and maximum shear stress in the region of blood flow monitored at each time step during one cycle are shown in Fig. 5(e) and Fig. 5(f). The time at which the maximum shear stress is observed is exactly the same as that of the maximum velocity. This time is identified to be in the end stage of the closing phase, and the magnitudes of both the maximum velocity and maximum shear stress are immensely larger. The maximum shear stress is quite a bit larger in the non-Newtonian case. This interpretation corresponds exactly with the account given before in association with Fig. 4.

CONCLUSIONS

The current study has numerically investigated blood flow through bileaflet mechanical heart valves. Here, the leaflet behavior associated with the blood flow has also been analyzed by using a fluid-structure interaction method. A finite volume computational fluid dynamics code and a finite element structure dynamics code have been used concurrently to solve the flow and structure equations, respectively, since the blood flow and leaflet motion are strongly coupled.

Two-dimensional, pulsatile blood flows have been simulated in valves with different maximum opening angles and blood has been assumed to be non-Newtonian and Newtonian fluid (with Carreau model). All calculations have been performed during one cycle of heartbeat. Flow fields, leaflet behavior, and shear stresses with time have been obtained and discharge flow rate and regurgitation flow rate have been calculated. In the end of the closing phase, the maximum shear stresses, an important issue for valve hemodynamic analysis, have been found around the leaflet and near the housing. The present research has shown the capability to describe the characteristics of the blood flow and leaflet motion, and to overcome the shortcomings of previous studies where the effect of leaflet motion has been ignored or approximated by simplified assumptions.

ACKNOWLEDGMENT

This study was financially supported by the Korea Research Foundation (Project number: KRF-99-042-F00127-F3300).

REFERENCES

Cerrolaza, M., Herrera, M., Berrios, R. and Annicchiarico, W., "A Comparison of the Hydrodynamical Behaviour of Three Heart Aortic Prostheses by Numerical Methods," *J. Medicine Engineering and Technology* (1997).

Chandran, J. B., "Pulsatile Flow Past a St. Jude Medical Bileaflet Heart," *J. Thorac. Cardiovasc. Surg.*, **89**, 743 (1985a).

Chandran, K. B., Cabel, G. N., Khalighi, B. and Chen, C. J., "Laser Anemometer Measurements of Pulsatile Flow Past Aortic Valve Prostheses," *J. Biomechanics*, **16**(10), 865 (1985b).

Chandran, K. M., Khalighi, B. and Chen, C. J., "Experimental Study of Physiological Pulsatile Flow Past Valve Prosthese in a Model of Human Aorta-. Tiling Disc Valves and the Effect of Orientation," *J. Biomechanics*, **18**(10), 773 (1985c).

Farahifar, D., Cassot, F. and Bodard, H., "Velocity Profiles in the Weak of Two Prosthetic Heart Valves Using a New Cardiovascular Simulator," *J. Biomechanics*, **18**(10), 789 (1985).

Fatemi, R. S. and Chandran, K. B., "An in Vitro Study of the St. Jude Medical and Edwards Duromedics Bileaflet Valve Using Laser Anemometry," *J. Biomech. Eng.*, **111**, 298 (1989).

Gokhale, V. V., Tanner, R. J. and Bischoff, K. B., "FE Solution for the Navier-Stokes Equations for a 2D Steady Flow through a Section of a Canine Aorta Model," *J. Biomechanics*, **11**, 241 (1978).

Gross, J. M., Shermer, C. D. and Hwang, N. H. C., "Vortex Shedding in Bileaflet Heart Valve Prostheses," *Trans. Am. Soc. Artif. Intern. Organs*, **34**, 845 (1988).

Hasenkam, J. M., Mygaard, H., Giersiepen, M., Reul, H. and Stodkilde-Jorgensen, H., "Turbulent Stress Measurements Downstream of Six Mechanical Aortic Valves in a Pulsatile Flow Model," *J. Biomechanics*, **21**, 631 (1988).

Imaeda, K. and Goodman, F., "Analysis of Non-linear Pulsatile Flow in Arteries," *J. Biomechanics*, **13**(8), 1002 (1980).

Jeong, Y. S. and Kang, I. S., "Pulsatile Flows in Stenosed Blood Vessels," *Korean J. Chem. Eng.*, **12**, 541 (1995).

King, M. J., "Computational and Experimental Studies of Flow through a Bileaflet Mechanical Heart Valve," Ph.D. Thesis. University of Leeds, UK (1994).

King, M. J., Corden, J., David, T., and Fisher, J., "A Three-Dimensional, Time-Dependent Analysis of Flow through a Bileaflet Mechanical Heart Valve: Comparison of Experimental and Numerical Results," *J. Biomechanics*, **29**(5), 609 (1996).

King, M. J., David, T. and Fisher, J., "An Initial Parametric Study of Fluid Flow through Bileaflet Mechanical Heart Valves Using Computational Fluid Dynamics," *J. Eng. Med.*, **208**, 63 (1994).

Krafczyk, M., Cerrolaza, M., Schulz, M. and Rank, E., "Analysis of 3D Transient Blood Flow Passing through an Artificial Aortic Valve by Lattice-Boltzmann Methods," *J. Biomechanics*, **31**, 453 (1998).

McQueen, D. M. and Peskin, C., "Computer-Assisted Design of But-

terfly Bileaflet Mechanical Heart Valves for the Mitral Position," *J. Comput. Fluids*, **82**, 289 (1985).

Nygaard, H., Paulsen, P. K., Hasenkan, J. M., Pedersen, E. M. and Rovsing, "Turbulent Stresses Downstream of Three Mechanical Aortic Valve Prostheses in Human Beings," *J. Thorac. Cardiovas. Surg.*, **107**, 438 (1994).

Rossean, E. P. M., Van de Ven A. P. C., Van Steenhoven, A. A. and Seroo, J. M., "Design of a System for the Accelerated Loading of Heart Valve Prostheses," *J. Biomechanics*, **17**(2), 145 (1984).

Sallam, L. A., Shaw, A. and Bain, W. H., "Experimental Evaluation of Mechanical Hemolysis with Starr-Edwards, Kay-Shiley and Bjork_ Shiley Valves," *Scan. J. Thorac. Cardiovas. Surg.*, **10**, 117 (1976).

Sikarskic, D. L., Stein, P. and Vable, M., "A Mathematical Model for Aortic Valve Vibration," *J. Biomechanics*, **17**(11), 831 (1979).

Skalak, R., "Finite Elements in Biofluid Mechanics. FE Analysis in Biomechanics," (1982).

Stevenson, D. M. and Yoganathan, A. P., "Numerical Simulation of Steady Turbulent Flow through Trileaflet Aortic Heart Valves-I. Computational Scheme and Methodology," *J. Biomechanics*, **18**(12), 899 (1985).

Swanson, W. M. and Clark, R. E., "Dimensions and Geometric Relationships of the Human Aortic Valve as a Function of Pressure," *Cir. Res.*, **35**, 871 (1974).

Thubrikar, M. J., Selim, G., Robicsek, F. and Fowler, B., "Effect of the Sinus Geometry on the Dynamics of Bioprosthetic Heart Valves (abstract)," *Ann. Biomed. Eng.*, **24**, S3 (1996a).

Thubrikar, M. J., Selim, G., Robicsek, F. and Fowler, B., "Effect of the Sinus Geometry on the Dynamics of Bioprosthetic Heart Valves (abstract)," Proceedings of the 18th Annual International Conference of the IEEE Engineering in Medicine and Biology Society, Amsterdam, The Netherlands, pg. 10 November (1996b).

Tillman, W., Reul, H., Herold, M., Bruss, K. H. and Van Gilse, J., "In Vitro Wall Shear Measurements at Aortic Valve Prostheses," *J. Biomechanics*, **17**(4), 263 (1984).

Woo, Y. R. and Yoganathan, A. P., "Pulsatile Flow Velocity and Shear Stress Measurements on the St. Jude Valve Prosthesis," *Scand. J. Thorac. Cardiovasc. Surg.*, **20**, 15 (1986).

Yang, H. Q. and Makhijani, V. B. "A Strongly Coupled Pressure-Based CFD Agroithm for Fluid-Structure Interaction," Proceeding of 32nd Aerospace Sciences Meeting and Exhibit, Reno, NV, AIAA-94-0719 (1994).

Yoganathan, A. P., Coreoran, W. H. and Harrison, E. C., "In Vitro Velocity Measurements in the Vicinity of Aortic Prostheses," *J. Biomechanics*, **12**, 135 (1979).